Electrothermal deterioration factors in gold planar inductors designed for microscale bio-applications

M. E. Rizou and T. Prodromakis

Electronic Materials & Devices Research Group, Zepler Institute, University of Southampton, University Road, SO17 1BJ, Southampton, UK

e-mail: m.rizou@soton.ac.uk, t.prodromakis@soton.ac.uk

Keywords: thermal degradation, planar micro-inductors, Joule heating, electromigration, microfabrication, micro-magnetic stimulation

Abstract

In this study, we present the fabrication of wafer level micro-inductors, designed for non invasive neuro-stimulation in vitro, along with an electrothermal study testing the influence of thermal phenomena to their performance. The electric performance of all micro-scale electromagnetic components is hampered by two dominant factors: Joule heating and electromigration. The scope of the study is to evaluate how these phenomena change the electric behaviour of the samples during activation. We experimentally define the safe area of operation across six types of samples with different geometric characteristics and we extract useful information for the reliability of the samples by comparing their median failure times. Our findings present the activation restrictions which should be taken into account in order to avoid the thermal degradation of the components, while at the same time could be used as design guidelines for similar geometries.

1. Introduction

The need of downscaling inductors in integrated circuits has been a long term requirement for a broad range of applications, while the development of microfabrication techniques has assisted towards this direction. In the majority of applications micro-coils are usually exploited in the radiofrequency (RF) range. Typical examples can be found in antenna applications, transformer designs [1,2], low noise amplifiers [3] and filters. In tandem, a number of different technologies [4] and geometries [5] have also been proposed in order to improve their performance and enhance their efficiency. Integrated inductors have also been used as sensors [6], in microscale NMR applications [7] and as transmitter-receiver systems for human body implants [8].

Recently the need of scaling down the size of the electromagnets is coming rapidly into the foreground in the field of bio-medical applications. In vitro, decreasing the size of the inductors is translated into high spatial resolution in either selectivity or sensing applications. At the same time, similar devices transferred to flexible substrates, could be used in vivo, serving the constantly growing need for devices implanted into living tissue. A bio-application which has attracted significant attention over the previous years is magnetic neuro-stimulation, which could be used as an alternative non-invasive method for exciting neural cells both in vitro [9,10] and in vivo [11,12]. The method is based on Faraday's law of induction and the idea was inspired by the clinical method of transcranial magnetic stimulation (TMS) [13,14], where an inductor is used to evoke activity on specific brain regions, used for treatment of different diseases. In vitro, the miniaturisation of TMS remains quite simple in principle, while it overcomes a series of problems that invasive techniques suffer from, such as the electrode corrosion, biofouling phenomena and electrode electrolyte interface problems. In vitro implementation of TMS demands a size of the inductor comparable to the size of the target cell, to assure a high spatial resolution and a localised region of activation. Up to now however, the inductors used were in the submillimetre scale as it is a challenge to achieve high spatial resolution and sufficient current capacity to trigger the cell activity without electrothermally wear out the inductors. The efficiency of a micro-magnetic stimulator to elicit cellular activity is defined by the geometric characteristics of the structure, the relative distance between the micro-inductor and a cell and by the maximum amplitude of the input current to the device.

Thermal and mechanical effects, such as Joule heating and electromigration, limit the performance of inductors especially when the cross section of the metallic components is decreasing to ~10μm^2. The thermal degradation of planar micro-inductors has been studied both experimentally [15], to identify the influence of the different substrates on the heat dissipation mechanism and numerically [16], in CMOS based inductors. The impact of these phenomena has been excessively studied on systems of very large scale integration interconnects (VLSI). More specifically, the flow of current through a metal conductor either for biasing or signal transmission purposes, is a means of power distribution to the system. However, a number of physical mechanisms transform the electrical power into thermal, influencing the design and reliability of the system. Circuit designers of large scale interconnect systems set restrictions to the maximum current density flowing into the system to eliminate as much as possible the increase of the temperature. [17–22].

For a time dependant current density j(t), two different quantities are involved in the deterioration mechanisms. The j_{rms} value is involved in the self-heating of the micro-coils, due to Joule heating, while the j_{avg} value is the involved in the electromigration mechanism [23]. Joule heating is a major issue of temperature increase in a metal and is described by equation 1.

$$\Delta \mathrm{T}_{\textit{Joule heating}} = T_m - T_{amb} = \mathrm{I}_{rms}^2 \ \mathrm{R}\,\mathrm{R}_{th} \quad (1)$$

T_m is the metal temperature, T_{amb} is the initial reference temperature, I_{rms} is the rms value of the flowing current, R is the electric resistance and finally R_{th} is the equivalent thermal resistance.

Electromigration is another temperature dependent phenomenon related to the mass transfer (metal atoms) due to high stress created as the current density increases. The main cause of the metal atoms mechanical movement is the momentum transfer from the electron wind. In some cases, the failure and damage caused are irreversible due to openings and loss of metal continuity. The phenomenon is more significant for DC currents, rather than AC currents of same magnitude. The median time to fail (MTF) in hours [24] is given by Black’s Law in equation 2.

$$MTF = \frac{A}{\mathrm{C}\,J^n}\ \mathrm{e}^{\frac{E_B}{kT_m}} \qquad (2)$$

Where A is the cross section, C is a constant depending the micro-structure of the deposited material, J is either the DC or average density in A/cm^2, n typically lies between 1-2, E_B is the activation energy in eV, k is the Boltzmann constant and T_m the temperature of the metal in degrees Kelvin.

The development of a neuro-stimulating tool able to work over a wide range of biological preparations and morphologies requires well defined limits of safe operation to add an additional level of control to our experiments. Within this study, we investigate the impact of both Joule heating and electromigration on the behaviour of our samples. We test the activation limits of the inductors, so as to define the maximum current density they could hold and we trigger a discussion on considerations which should be taken into account in the design of similar type electromagnets. The chip we propose for magnetic stimulation of neural cells in vitro consists of 36 micro-inductors in a square array and is developed with standard micro-fabrication techniques. Six different geometries are studied, all of which with a side width of 100µm, but with differences in the metal track width and thickness.

2. Materials and Methods

2.1 Microfabrication of a planar inductors

The fabrication procedure is illustrated in figure 1 (a). The use of a ground plane to connect the one end of the micro-coils was chosen based on a number of different reasons. The ground plane is made of Au and is deposited by an electron beam evaporator in the thickness of 50nm, which corresponds to a sheet resistance of 488mΩ/square. The ground plane simplifies the configuration in the two dimensional array, as every coil will need a single pad connection instead of two. It also enables all the metallic structures to be galvanically connected to the same potential during the electroplating step. Between the silicon wafer and the electrodeposited layer of Au, a Cr layer of 5nm is added for adhesion purposes. With reactive sputtering a 100nm thick insulating layer of SiN is then deposited. Optical lithography is used to create the vias to the ground plane (1st optical lithography) and the metallic track of the micro-coils (2nd optical lithography), in combination with inductively coupled plasma etching of SiN and lift off of Au (100nm) respectively.

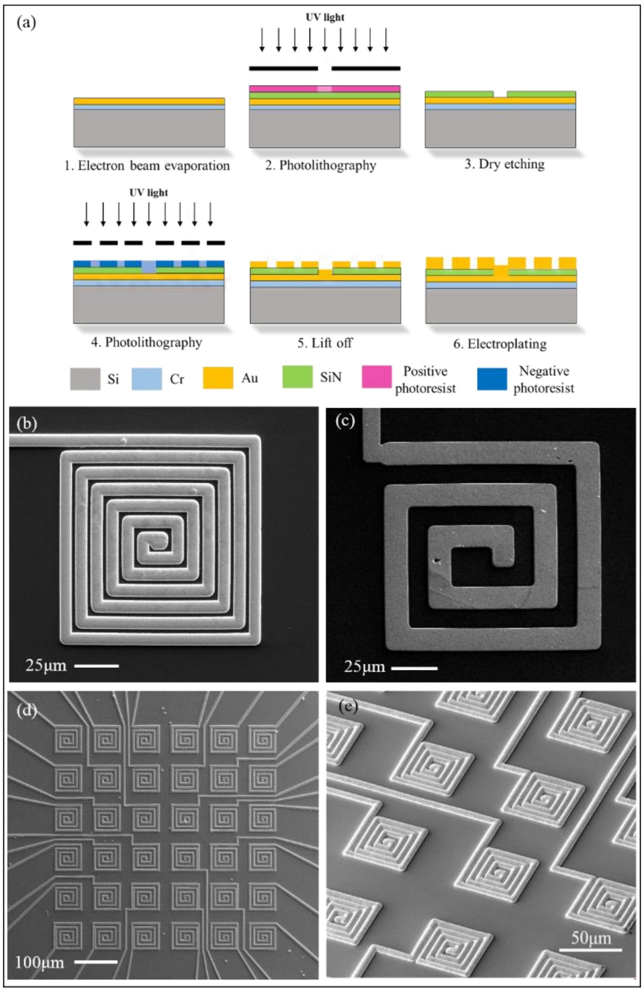

Figure 1. (a) Schematic graph with the fabrication steps in the development of a micro-coil. **(b), (c)** SEM images of fabricated planar micro-inductors (samples I, VI respectively). **(d), (e)** SEM images of a fabricated 6x6 array.

Electroplating is finally used to increase the micro-coils' thickness to the micro-scale. The results presented below concern micro-coils with a thickness of 0.9μm and 1.95μm. The characteristics of the structures under study as well as the DC resistance of each micro-inductor are summarised in table 1 below. All the micro-coils cover an equal surface area of 100x100μm^2, chosen for adequate spatial resolution within the cell culture area. Imaging with a scanning electron microscope (SEM) of single coil geometries and array configurations fabricated are also illustrated on figure 1 (b), (c).

2.2 Measurement procedure

The measuring procedure followed involves a DC current set as an input, with a constantly increasing amplitude from 1-100mA. Between each amplitude step and after a significant time waited for thermal equilibrium, another DC value of lower amplitude is applied, at 1mA, representing a measurement in a colder state of a micro-coil. All the measurements were performed with a current list sweep on Keithley 4200C semiconductor parameter analyser, in a pulsed mode, where the duration of the ON and OFF phases of each pulse lasted 100ms and 1s respectively. The choice of 1s as a safe time for the system to reach equilibrium was tested prior to our actual experiment, with some parametric testing. Since we were not aware for the time constant of our system, our initial measurements started with a current list sweep with 10ms of pulses followed by 10s of rest. Our measurements were compared with pulses of 10ms followed by 5s of rest and finally 10ms on and 1s of rest. Since no significant differences were observed in the behaviour of the samples in the different cases, we considered 1s as a safe limit for the system to reach equilibrium and study the steady state. We tried both a forth and back pulse sweep, as part of the experiment standardisation in the first steps of our study. For measurements below the deterioration limit, we did not observe any non-linear effect and this is why we decided to focus on measurements of increasing amplitude pulses only. Above the deterioration limit, the backward measured values (especially of R_{cold}) became more random, a fact which was considered as an indication of deterioration of the device.

The settings are chosen to be equivalent to those needed in a realistic scenario of excitable cells' excitation. The rms values of the current density are determined by the choice of the specific duty cycle (10%), which is based on the worst case scenario of a realistic activation scheme. Keeping a record of the resistance, obtained from current and voltage values, in the hot and cold states of the micro-coils enables us to calculate the T_{hot} and T_{cold} temperature in every step and finally plot the power injected and dissipated by the micro-coils over temperature. Specifically T_{hot} and T_{cold} are calculated from equations 3 and 4 at every measurement point. The DC resistance of the inductor is given by equation 3, where ρ_T is the electric resistivity of the material, l is the total length and S the surface which corresponds to the cross section of the metallic track.

$$R=\rho_T \frac{l}{S} \qquad (3)$$

The electric resistivity ρ_T depends on the temperature in a linear manner, as expressed by equation 4. P_{Tamb} is the resistivity at ambient temperature with a value of 2.44 10^{-8} Ohm·m for gold and a_{th} is a temperature coefficient, which for gold has the value of 0.0034K^{-1}.

$$\rho_T = \rho_{T_{amb}} \left(1+\alpha_{th}\left(T-T_{amb}\right)\right) \qquad (4)$$

The measurements are performed with a 2 probe setup. One SMU in current mode feeding the inductor through the biasing pad and the other SMU forcing a reference zero potential in the ground pad (current list sweep in pulsed mode). The resistance value is obtained from the voltage measured with a resolution of 1μV and set current.

3. Results

3.1 Effects of Joule heating in electric resistance

The deterioration points of the six different geometries are illustrated on figure 2 a,b. Samples I-III are geometries with different track width from a die with thickness 1.95μm, while IV-VI are similar geometries with lower thickness, 0.9μm. The geometric characteristics of the samples are summarized in Table 1. Every two measurements (one hot at different current and one cold constantly at 1mA) the biasing current increases by 1mA. For each coil, the upper and lower set of measurements correspond to the hot and cold measurements respectively. The resistance is plotted along the number of measurements, so as to illustrate clearly the behaviour of the resistance at the colder states. However it remains easy to correlate each number of hot measurement to the current flowing through the micro-coil, since: I(mA)= #measurement/2+0.5. For example, coil I reveals a deterioration point at #measurement 89, which corresponds to I(mA)=89/2+0.5=45mA. Samples III and VI, have a deterioration limit at current amplitudes greater than the maximum 99mA we tested. The resistance is extracted based on measurements of two different micro-coils of the same geometry. As expected the smaller the metallic track cross section of a micro-coil, the lower the current at which the degradation occurs. This is obvious either by comparing different geometries on the same thickness (eg. samples I-III versus IV-VI), or same geometries over different thickness (eg. samples I versus IV). The behaviour of sample IV is revealing the expected behaviour with some more stochasticity, which could be attributed to the fact that it is the most sensitive geometry. Sample IV has the smallest cross section in comparison to the rest of the samples. The values of resistance before starting the current sweep, are presented also in Table 1, along with their expected values, which were calculated analytically.

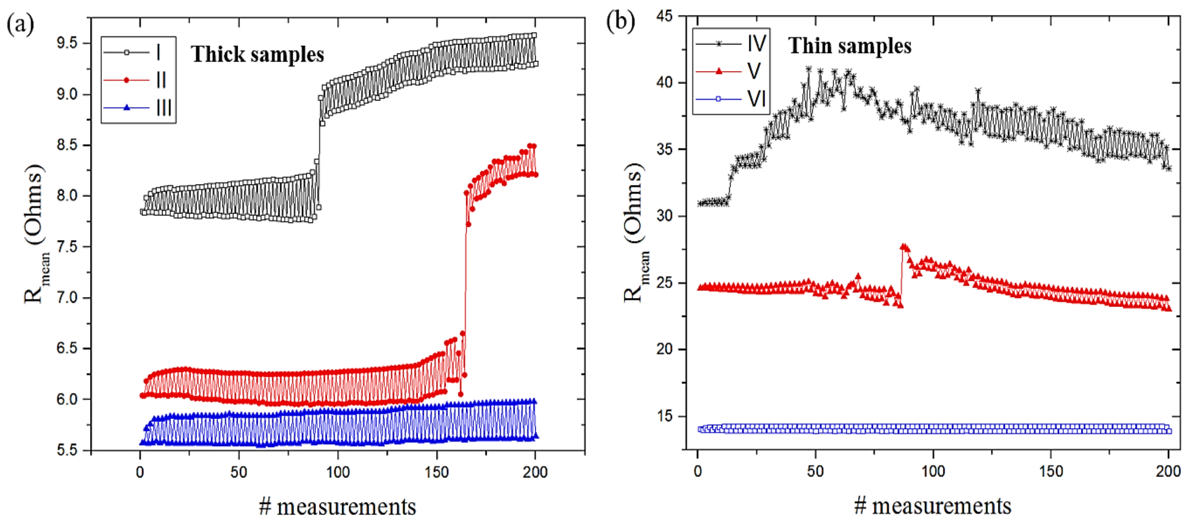

Figure 2. Thermal degradation of micro-coils, given by a steep increase in resistance as the current increases. **(a)** Samples I-III with a thickness of 1.95μm and **(b)** Samples IV-VI with a thickness of 0.9μm.

Sample	Thickness (μm)	Width (μm)	R_{calc} (Ohms)	$R_{cold\text{-}meas} \pm \delta R_{cold}$ (Ohms)	I_{det}(mA)
I	1.95	5.9	8.16	7.85±2.53	45
II	1.95	8.9	4.32	6.04±2.50	80
III	1.95	13.9	3.69	5.56±2.15	>99
IV	0.90	3.8	25.72	30.17±4.73	24
V	0.90	6.8	11.93	27.20±6.67	40
VI	0.90	11.8	6.61	14.03±4.27	>99

Table 1. Geometric characteristics, electric resistance and current (peak values) at deterioration point of the geometries under study.

The value of the resistance arises from the micro-coil resistance, which is standard for all micro-coils in an array, plus some additional factors. The additional factors are the resistance from the thin wire which connects the coil to the pad and the influence of electroplating on the geometric characteristics. Part of the thin wire geometry is illustrated on figure 1 (d),(e). The thin wire has a mean length value of 2000μm and differs up to ≈300μm between different coils within the same array. In the case of an electrodeposited layer of Au with a thickness of 1.95μm, this is translated as an additional resistance in the order of 0.2Ohms/100μm. This is also taken into account as a systematic error on the estimation of the resistance uncertainty. The δR_{cold} error includes both the standard error of two measurements in different coils of same type and also a systematic factor arising from the thin wire difference in length.

3.2. Heat transfer mechanisms and maximum current density at the deterioration point

The electric energy applied to the devices is converted to thermal and figure 3 shows the change of temperature over the applied power. The non-linear behaviour of the graph indicates that heat is not only dissipated by thermal conduction, but also by additional heat transfer mechanisms, such as convection. Figure 3 shows the results for the thick and thin structures. The power is calculated from the measured voltage and current values and is plotted up to 75mW.

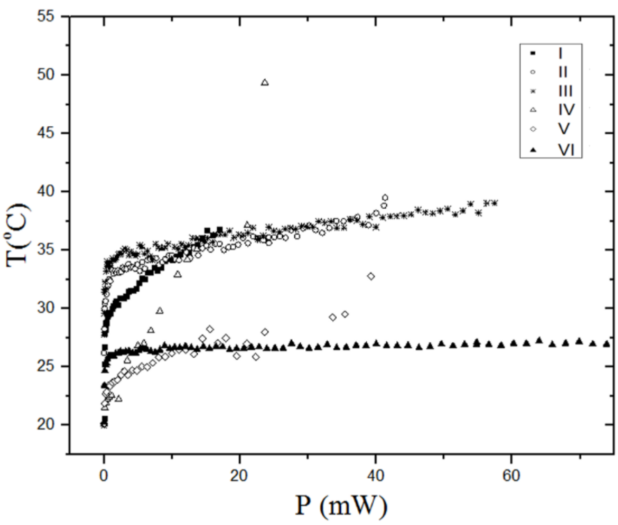

Figure 3. Temperature over applied power for the six geometries.

The rms current density up to the deterioration point of each sample is presented in figure 4. A linear fit of the deterioration points of the structures, illustrated as red full circles in figure 4, is giving a relation between the maximum current density flowing to the different geometries and the deterioration temperature. Sample IV was excluded from the fit, so as to obtain a more accurate result. Being the most sensitive sample, in the sense of thiner cross section, reveals the most unstable and noisy behaviour between all samples especially as it approaches the deterioration point. This is also obvious from figure 2(b). More specifically, the extrapolated relation is presented below.

$$J_{rms|\det}\left(\frac{mA}{\mu m^2}\right) = -\,0.133 T_{\det}\left({}^{o}C\right) + 6.345 \qquad (5)$$

Figure 4 and expression 5, provide key information for the design of micro-inductors as inductive components or heating elements.

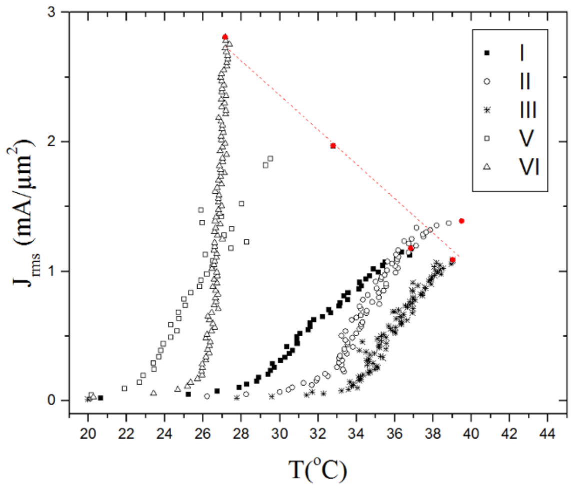

Figure 4. The current density (rms values) of the geometries versus the temperature of the metal due to Joule heating. The deterioration points are plotted as red full circles.

3.3 Long term reliability analysis: electromigration

Embedding the magneto-stimulating platform into a lab on a chip device is translated into a need for long term functionality. However, electromigration is another deterioration factor which affects the long term reliability of the micro-coils and should be taken into consideration. As discussed, Black's law, in equation 3, describes the failure time of electronic components functioning at specific conditions. However, in our case it is not possible to estimate the value of the constant C as it is related to specific characteristics of the electroplated gold layer, such as the metal grain size. At the same time, there is no scientific record for the value of this constant for gold, as most of the studies focus on standard materials used in CMOS technologies. Even though it is not possible to calculate an absolute value for the MTF of each sample in our case, we make a relative comparison between the samples. The MTF of each sample is calculated in respect to the MTF of the most sensitive sample in terms of geometry, which is the IV sample. This will enable us to find the most reliable amongst the samples and also quantify its superior performance. Assuming functionality of the inductors close to their deterioration limit, with a duty cycle as above and under non-stop functionality, we study the worst case scenario. For the calculation we use the current density at the deterioration point of each sample, the temperature is given from the relation $T_m=T_{ref}+\Delta T_{det}$, where T_{ref}=293K and ΔT_{det} arises from the previous Joule heating study and represents the increase of temperature at the deterioration point. Finally, the activation energy of an electroplated and not passivated gold layer is E_a=0.88eV [25]. Figure 5 summarizes the comparison of the MTF of each sample over the MTF of sample IV. As expected, all samples have higher MTF, with sample III revealing the highest with MTF_{III}/MTF_{IV}=83.53±28.96. Electromigration should also be taken into account in case there is a demand (eg. arising from the biological experiment) for increasing the current flowing through the micro-coils. In that case, the duty cycle of the train of pulses becomes an important factor. More specifically, the MTF should be higher than or equal to a failure time set as a goal, described by equation 6.

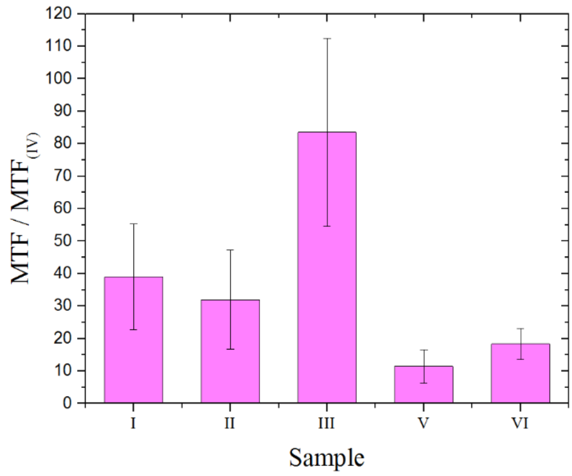

Figure 5. The median time to fail (MTF) of each sample over the MTF of the sample IV, with the smaller cross section.

$$MTF \geq MTF_{goal} \Rightarrow \frac{\exp\left(\frac{E_a}{kT_m}\right)}{J_{avg}^2} \geq \frac{\exp\left(\frac{E_a}{kT_{ref}}\right)}{J_o^2} \qquad (6)$$

Where T_{ref}=293K and J_o is the current density at the deterioration point. Since $J_{avg}=r\cdot J_{peak}$, the peak value of the allowed current density at a specific temperature Tm, is bound by the upper limit of equation 7.

$$J_{peak}^2 \leq \frac{J_o^2}{r^2} \frac{\exp\left(\frac{E_a}{kT_m}\right)}{\exp\left(\frac{E_a}{kT_{ref}}\right)} \qquad (7)$$

Plotting this relation in figure 6, for sample IV, shows how drastically the maximum allowed current density peak decreases in higher metal temperatures. At the same time, the plots of different duty cycles indicate that towards spike operation micro-coils could sustain higher amounts of current, if this is needed for stimulation purposes. The relation is plotted over a biologically acceptable temperature range since temperatures above 40°C cannot be tolerated due to cell sustainability reasons.

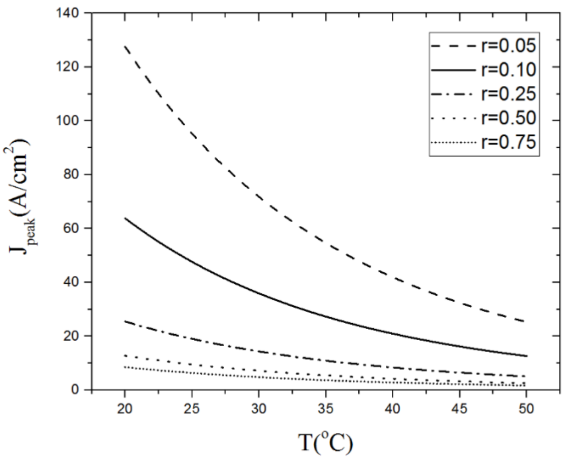

Figure 6. The maximum allowed peak value of current density pulses over the metal temperature T_m, for five different duty cycles (sample IV).

4. Conclusions

In this article we presented the fabrication of planar inductors made of gold on a silicon wafer, designed as the key component to a platform of magnetic stimulation of excitable cells in vitro. The main scope of the study was firstly to identify the limits of safe operation of different geometries under functioning conditions similar to those needed in a real bio-experiment. A relation between the current density at the deterioration limit and the temperature was also extrapolated and could act as a design parameter to similar studies. Finally, the effect of electromigration on the samples was also an interest of this study. A comparison of the different median failure times was presented along with the calculation of the maximum allowed current density peak value for different duty cycles. In conclusion, our findings presented the factors of electrothermal deterioration and design considerations important for the implementation of a high-spatial resolution micro-magnetic array into a biocompatible prototype for non-invasive cell stimulation.

Acknowledgements

We would like to acknowledge the financial support of the A.G. Leventis Foundation.

References

[1] K. Chong, Y.H. Xie, High-performance on-chip transformers, IEEE Electron Device Lett. 26 (2005) 557–559. doi:10.1109/LED.2005.851817.

[2] H. Jiang, Z. Li, N.C. Tien, Reducing Silicon-Substrate Parasitics of on-Chip Transformers, 15th IEEE Int. Conf. Micro Electro Mech. Syst. (2002) 649–652. doi:10.1109/MEMSYS.2002.984354.

[3] Y. Jeong, H. Doh, S. Jung, D.S.W. Park, J.B. Lee, CMOS VCO & LNA implemented by air-suspended on-chip RF MEMS LC, in: 47th IEEE Int. Midwest Symp. Circuits Syst., 2004: pp. 373–376.

[4] M. Rais-Zadeh, F. Ayazi, Characterization of high- *Q* spiral inductors on thick insulator-on-silicon, J. Micromechanics Microengineering. 15 (2005) 2105–2112. doi:10.1088/0960-1317/15/11/016.

[5] C.L. Chua, K. Van Schuylenbergh, J.-P. Lu, D.K. Fork, High-Q RF coils on silicon integrated circuits, MEMS Components Appl. Ind. Automob. Aerospace, Commun. II,. 4981 (2003) 150. d:%5Cstudy/RF/papers/High-Q RF coils on silicon integrated circuits.pdf.

[6] S. Tumanski, Induction coil sensors-a review, Meas. Sci. Technol. 18 (2007) R31–R46. doi:10.1088/0957-0233/18/3/R01.

[7] C. Massin, G. Boero, F. Vincent, J. Abenhaim, P.-A. Besse, R.S. Popovic, High- Q factor RF planar microcoils for micro-scale NMR spectroscopy, Sensors Actuators A Phys. 98 (2002) 280–288. http://www.sciencedirect.com/science/article/pii/S0924424701008470 (accessed October 20, 2014).

[8] C.R. Neagu, H.V. Jansen, A. Smith, J.G.E. Gardeniers, M.C. Elwenspoek, Characterization of a planar microcoil for implantable microsystems, Sensors Actuators A Phys. 62 (1997) 599–611. doi:10.1016/S0924-4247(97)01601-4.

[9] G. Bonmassar, S.W. Lee, D.K. Freeman, P. Miloslav, S.I. Fried, J.T. Gale, Microscopic magnetic stimulation of neural tissue, Nat. Commun. 3 (2012) 921. doi:10.1038/ncomms1914.

[10] S.W. Lee, S.I. Fried, Suppression of Subthalamic Nucleus Activity by Micromagnetic Stimulation, IEEE Trans. Neural Syst. Rehabil. Eng. 23 (2015) 116–127.

[11] H.J. Park, G. Bonmassar, J.A. Kaltenbach, A.G. Machado, N.F. Manzoor, J.T. Gale, Activation of the central nervous system induced by micro-magnetic stimulation., Nat. Commun. 4 (2013) 2463. doi:10.1038/ncomms3463.

[12] S.W. Lee, F. Fallegger, B.D.F. Casse, S.I. Fried, Implantable microcoils for intracortical magnetic stimulation, Sci. Adv. 2 (2016) e1600889–e1600889. doi:10.1126/sciadv.1600889.

[13] A.T. Barker, R. Jalinous, I.L. Freeston, Non-Invasive Magnetic Stimulation of Human Motor Cortex, Lancet. 325 (1985) 1106–1107. doi:10.1016/S0140-6736(85)92413-4.

[14] L.L. Herrmann, K.P. Ebmeier, L.L. Hermann, K.P. Ebmeier, Transcranial magnetic stimulation, Psychiatry. 5 (2006) 204–207. doi:10.1016/j.mppsy.2009.01.008.

[15] J. Moulin, M. Woytasik, J.-P. Grandchamp, E. Dufour-Gergam, A. Bosseboeuf, High current densities in copper microcoils: influence of substrate on failure mode, in: Current, Stresa, Italy, 2006: pp. 26–28.

[16] F. Reverter, T. Prodromakis, Y. Liu, P. Georgiou, K. Nikolic, T. Constandinou, Design considerations for a CMOS Lab-on-Chip microheater array to facilitate the in vitro thermal stimulation of neurons, IEEE Int. Symp. Circuits Syst. (2014) 630–633. doi:10.1109/ISCAS.2014.6865214.

[17] W.R. Hunter, Self-consistent solutions for allowed interconnect current density-part I: Implications for technology evolution, IEEE Trans. Electron Devices. 44 (1997) 304–309. doi:10.1109/16.557721.

[18] P.K. Chatterjee, W.R. Hunter, A. Amerasekera, S. Aur, C. Duvvury, P.E. Nicollian, L.M. Ting, P. Yang, Trends for Deep Submicron, in: Proc. IRPS, 1995: pp. 1–11.

[19] T.Y. Chiang, K. Banerjee, K.C. Saraswat, Analytical thermal model for multilevel VLSI interconnects incorporating via effect, IEEE Electron Device Lett. 23 (2002) 31–33. doi:10.1109/55.974803.

[20] S. Kilgore, C. Gaw, H. Henry, Electromigration of electroplated gold interconnects, MRS Proc. 863 (2005) 1–6. doi:10.1557/PROC-863-B8.30.

[21] B.K. Liew, N.W. Cheung, C. Hu, Projecting Interconnect Electromigration Lifetime for Arbitrary Current Waveforms, IEEE Trans. Electron Devices. 37 (1990) 1343–1351. doi:10.1109/16.108197.

[22] S. Rzepka, K. Banerjee, E. Meusel, C.H.C. Hu, Characterization of self-heating in advanced VLSI interconnect\nlines based on thermal finite element simulation, IEEE Trans. Components, Packag. Manuf. Technol. Part A. 21 (1998) 406–411. doi:10.1109/95.725203.

[23] K. Banerjee, A. Mehrotra, A. Sangiovanni-Vincentelli, C. Hu, On thermal effects in deep sub-micron VLSI interconnects, in: Proc. 1999 Des. Autom. Conf. (Cat. No. 99CH36361), 1999: pp. 885–891. doi:10.1109/DAC.1999.782207.

[24] J. Black, Electromigration—A brief survey and some recent results, Electron Devices, IEEE Trans. 16 (1969) 338–347. doi:10.1109/T-ED.1969.16754.

[25] A. Gangulee, F.M. d'Heurle, The activation energy for electromigration and grain-boundary self-diffusion in gold, Scr. Metall. 7 (1973) 1027–1030. doi:10.1016/0036-9748(73)90007-0.